Bull Volcanol (1996) 57:587–601

ORIGINAL PAPER

N. S. Bagdassarov · D. B. Dingwell · M. C. Wilding

Rhyolite magma degassing: an experimental study of melt vesiculation

Received: March 20, 1995 / Accepted: October 24, 1995

Abstract The vesiculation of a peralkaline rhyolite melt (initially containing ~0.14 wt.% H_2O) has been investigated at temperatures above the rheological glass transition ($T_g \approx 530$ °C) by (a) in situ optical observation of individual bubble growth or dissolution and (b) dilatometric measurements of the volume expansion due to vesiculation. The activation energy of the timescale for bubble growth equals the activation energy of viscous flow at relatively low temperatures (650–790 °C), but decreases and tends towards the value for water diffusion at high temperatures (790–925 °C). The time dependence of volume expansion follows the Avrami equation

$$\Delta V(t) \sim \{1 - \exp[-(t/\tau_{av})^n]\}$$

with the exponent $n = 2$–2.5. The induction time of nucleation and the characteristic timescale (τ_{av}) in the Avrami equation have the same activation energy, again equal to the activation energy of viscous flow, which means that in viscous melts (*Peclet* number < 1) the vesiculation (volume expansion), the bubble growth process, and, possibly, the nucleation of vesicles, are controlled by the relaxation of viscous stresses. One of the potential volcanological consequences of such behavior is the existence of a significant time lag between the attainment of a super-saturated state in volatile-bearing rhyolitic magmas and the onset of their expansion.

Key words Rhyolite · Vesiculation · Kinetic · Water · Diffusion · Degassing

Editorial responsibility: J. H. Fink

N. S. Bagdassarov (✉)[1] · D. B. Dingwell · M. C. Wilding[2]
Bayerisches Geoinstitut, Universität Bayreuth,
D-95440 Bayreuth, Germany

Present addresses:
[1] Institut für Meteorologie und Geophysik,
J. W. Goethe-Universität Frankfurt, D-60323 Frankfurt/M., Germany
[2] Geological and Geophysical Sciences,
Princeton University, Princeton, NJ 08544, USA

Introduction

The rate of the vesiculation process is an important factor controlling the physics of silicic volcanism. Explosive or effusive eruptive activities associated with magmatic degassing are directly linked with the intensity of magma vesiculation, the rate of its decompression, and volume expansion. Even if magma has degassed at a slow rate (due to a high viscosity), its volume expansion may generate dangerous volcanic blasts. For example, when a volatile-bearing magma is exposed to the shock release of hydrostatic pressure (through the collapse of the volcanic edifice or from tectonic movement) the resulting disintegration of melt into shards may cause significant destruction of the surrounding area (e.g. Shimozuru 1991; Fink 1992; Fink and Kieffer 1993) with profound environmental and economic implications. Thus, one of the central questions of volcanology is whether it is possible to predict the likelihood of effusive vs explosive eruptions on the basis of the physical properties of magmas such as rheology, volatile content, and rate of volatile exsolution (Fisher and Schmincke 1984).

The physical understanding of delayed expansion, bursting and disaggregation of silicic magmas/lavas requires studying the separation of gas from melt in highly viscous liquids (with shear viscosity $\eta > 10^7$ Pa s). The present work addresses the kinetic aspects of this problem with a study of the vesiculation of rhyolite melt using dilatometric and in situ optical means.

We describe the vesiculation process of magmas in terms of the gas-melt separation, i.e. the vapor phase nucleation and subsequent growth of vapor bubbles. The kinetics of degassing, or the rate of volume expansion $V(t)$ of the gas-melt aggregate, is determined by the superposition of two time-dependent processes: (a) the nucleation rate $J(t_1)$ (number of nuclei per unit of

volume per second generated in the time interval $[t_1, t_1+\mathrm{d}t]$, and (b) the volumetric growth rate of these vesicles over time period $[t-t_1, t]$: $V_\mathrm{b}(0)\, V_\mathrm{b}'(t-t_1)$ (volume per second), where $V_\mathrm{b}(0)$ is the initial volume of a newly nucleated bubble, $V_\mathrm{b}'(t)$ is a bubble growth rate (1/s). The total effect of the volume expansion is

$$V(t) = V_0 \int_0^t J(t_1) \left[\int_0^{t-t_1} V_\mathrm{b}(0)\, V_\mathrm{b}'(t)\, \mathrm{d}t_2 \right] \mathrm{d}t_1 \propto \int_0^t J(t_1) [\mathrm{V}_\mathrm{b}(t-t_1) - V_\mathrm{b}(0)]\, \mathrm{d}t_1 \quad (1)$$

The physical meaning of Eq. (1) can be understood by analogy with the volume rate of crystallization (Kirkpatrick 1976) assuming that (a) the initial volume of melt (V_0) itself does not change significantly during the gas separation, and (b) the initial volume of nuclei (volume $V_\mathrm{b}(0)$ of an embryo of a critical size) present in the liquid can be ignored in comparison with the volume of expanded gas. The volumetric effect of magma degassing may be estimated using Eq. (1), if the nucleation rate of vesicles $J(t)$ and the volumetric growth rate of individual vesicles $V_\mathrm{b}'(t)$ can be determined from laboratory experiments. The time dependence $J(t)$ and $V_\mathrm{b}(t)$ can also be obtained from general theoretical considerations assuming some mechanism of bubble growth. Here in we address the physical background of delayed phase separation and the growth process of gas bubbles in viscous liquids.

The first cause for the delay in degassing of viscous melts stems from the character of bubble nucleation. The rate of bubble nucleation during the phase separation $J(t)$ can be steady state or transient (resulting in a delayed nucleation process). The driving force for nucleation (the amplitude of the nucleation rate function) is an exponential function of the degree of supersaturation and of the mobility of the species forming the new phase. In the case of viscous liquids the restricted mobility of species can result in delaying effects of phase separation. In laboratory experiments with melts, the nucleation rate function $J(t)$ always decays with time (Murase and McBirney 1973) because the volume available for progressive nucleation remains constant and the degree of supersaturation decreases with time. Until a steady-state distribution of cluster size is attained, the rate of nucleation may be time dependent. The influence of long-range diffusion of a species results in a delay between the start of supersaturation and the onset of steady-state nucleation (constant rate of nucleation J_0). The characteristic timescale of this process τ_ind is called the induction time (Kashchiev 1969) or the lag time (time delay) and characterizes "… the capacity of the system to reorganize itself until a steady state flux of nuclei is produced" (Toschev 1973). The induction time for the nucleation process in viscous media (media with limited mobility of diffusing species) may be estimated as $\tau_\mathrm{ind} \sim [D\,\Delta H(t)^2]^{-1}$, where D is the diffusion coefficient of the species separating in two phases, and $\Delta H(t)$ is a time-dependent degree of supersaturation. For the case of water separation from a highly viscous melt both species (molecular water and OH^- groups) contribute to the nucleation process and, thus, the "effective diffusivity" of both of them may be taken as D, which is in fact much lower than the diffusivity of molecular water (Jambon et al. 1992). In general, the diffusivity of chemical species D relates to the shear viscosity η via the Stokes-Einstein relationship $\eta D \propto \mathrm{T}$. It implies that both η and D have an Arrhenius temperature dependence as function of T with nearly the same activation energy. In the case of water diffusion in viscous melts and glasses the empirical relationship between diffusivity and shear viscosity is $D\,\eta^m = \mathrm{const}$, where m is an empirical constant. The parameter m is a ratio of the activation energy for the diffusion to that for the viscous flow. In the case of silica glass and low concentration of water $m = 1/8$ for OH^- group diffusion, with the increase of molecular water content $m \Rightarrow 1$ (Burn and Roberts 1970). Also, in felsic melts the parameter m significantly depends on what kind of diffusing species dominates in the total flux of water. At low viscosities (high temperatures, total water content >1 wt.%) the effective mobility of water can be scaled by the shear viscosity of the melt $D \propto 1/\eta$ (e.g. Thomas 1994) and at high viscosities (low temperature, low water content ≈ 0.1 wt.%) $D \propto 1/\eta^{1/8}$ (Jambon et al. 1992). Thus, the induction time and the kinetics of water separation from the viscous rhyolite melt may vary differently with temperature for low vs high water contents. If the total amount of dissolved water is high ($\gg 1$ wt.%), the dominant species of dissolved water is molecular water which possesses a relatively high diffusivity. At low total water concentrations the water is dissolved mostly as OH^- species and the escape of water from the melt consists of two processes. First, the small amount of molecular water escapes relatively quickly into a vapor phase (bubbles). Then, due to slow exchange kinetics of OH^- and molecular water, the bulk water diffusion is significantly delayed (Jambon et al. 1992) and bubbles nucleated from molecular water grow relatively slowly following the rate of conversion of OH^- groups to molecular water.

The expression for the induction time scale indicates that this lag time should be observable only for slowly diffusing species, i.e. in highly viscous media ($\eta \sim 10^9$ Pa s), such as for silica-rich magmas at temperatures slightly above their glass transition. In silicate melts diffusion coefficients of volatile species depend on temperature, composition, and concentration, and may be as low as $\sim 10^{-8}$ cm^2/s for molecular water (e.g. Zhang et al. 1991) and 10^{-10} cm^2/s for OH^- species at 700–650 °C (Jambon et al. 1992). Thus, depending on the temperature and degree of supersaturation, the lag time for bubble nucleation may be observed on a laboratory timescale. In the temperature interval near the glass transition the lag time of nucleation plus the delayed kinetics of water interconversion (if the total amount of water is $\ll 1$ wt.%) contributes substantially

to the time delay of the volume expansion during foaming experiments. In the process of magma cooling the transient nucleation may be coupled with changes in the degree of supersaturation $\Delta H(t)$ and the variation of the effective diffusion coefficient D. In this case the final size distribution of vesicles in magmas is difficult to interpret (c.f. Toramaru 1989; Bottinga and Javoy 1991; Mangan et al. 1993). The size distribution of bubbles may be affected in such situations by the complex mechanism of water-melt separation. Moreover, in some cases where the diffusion of separating species is very slow, at viscosities $>10^7$ Pa s the process of phase separation can be completed before the steady state is established (Toschev 1973). All this means that the steady-state nucleation rate J_0 may be unattainable during water separation from silica-rich melts at low concentrations of water (c.f. Hurwitz and Navon 1994).

The first experiments on the bubble nucleation rate in rhyolite melt (Murase and McBirney 1973) indicated that the shape (skewness) and the characteristic timescale of $J(t)$ depends on temperature. Differences in viscosity of about two orders of magnitude corresponded to two orders of magnitude difference in $J(t)$ at temperatures between 1050 and 950 °C (see Fig. 36 in Murase and McBirney 1973).

More recently, the nucleation process of a vapor phase in a magmatic melt has been studied by quenched time series experiments on annealed rhyolite glasses at 1 bar and high temperature (Bagdassarov and Dingwell 1993), and in quenched experiments at high pressure using the decompression of a water-saturated rhyolite melt (Hurwitz and Navon 1994). These results show that homogeneous nucleation is unlikely. Surfaces of some crystalline phases are the most likely sites of heterogeneous nucleation because they can potentially generate areas slightly enriched in water due to its exclusion from anhydrous crystals (Bagdassarov and Dingwell 1993).

The second reason for the delayed gas separation in viscous melts is the delayed character of the bubble growth itself. The main reason for this is the nonuniform initial concentration profile around nucleated bubbles and the mechanical relaxation of their shape. In general, the time dependence of a bubble growth $V_b(t)$ is a solution of two coupled equations of momentum and mass transfer (Cable and Frade 1994). Depending on whether or not the mass transfer on the vesicle interface is taken into account, there are two models of diffusional and expansional bubble growth.

The analysis of diffusional growth for individual bubbles in infinite space (Scriven 1959; Sparks 1978) indicates parabolic radius growth with time $R(t) \propto \sqrt{Dt}$. That solution is based on the assumption that the volume available for the diffusion of gas into a bubble is infinite, viscous retardation effects can be neglected, and the pressure increase inside the bubble does not significantly affect the boundary condition for the solubility on the bubble interface. The initial concentration profile around the bubble is assumed to be uniform. Moreover, it is appropriate for the case of an ideal gas dissolved in a low viscosity liquid (where diffusion of gas species is relatively fast and there are no delaying effects such as chemical reactions during the process of gas separation). If a large population of bubbles grow diffusionally and their boundaries do not interact mechanically with each other, at later stages of the vesiculation process the average size of the population of bubbles and the broadness of the size distribution increases proportionally to the diffusion coefficient of the separating vapor species (Lemlich 1978; Toramaru 1989).

When a volume available for the diffusion of gas into a bubble is restricted by a thin spherical shell, numerical modeling of bubble growth reveals that the time dependence of $V_b(t)$ is more complicated than given by the parabolic law (Arefmanesh et al. 1990; Arefmanesh and Advani 1991; Cable and Frade 1994). This numerical modeling is based on the solution of two coupled equations of mass and momentum transfer. The method has been compiled for the case of magmatic melts (Proussevitch et al. 1993) and the results demonstrate a noticeable deviation from the parabolic law (see the discussion between Sparks 1994 and Sahaganian et al. 1994). At low viscosities ($<10^6$ Pa s) there is a short period of time when the bubble growth may be regarded as parabolic. Then it changes until all volatiles have been diffused into the bubble, the growth rate then decaying and the dependence of bubble size as a function of time describing a sigmoidal shape. The time period of parabolic growth is practically unobservable for rhyolite melt compositions where viscosity is $>10^{6-7}$ Pa s.

For pure expansional bubble growth when diffusion of gas into a bubble is neglected and the growth is only due to the overpressure (ΔP) inside a bubble, the characteristic time scale of growth is $\tau_{gr} \approx \eta/\Delta P$ (Sparks et al. 1994). Thus, the time scale of bubble growth in viscous liquids can be analyzed on the basis of the Peclet (Pe) number.

$$Pe = \frac{\Delta P R^2}{\eta D} \tag{2}$$

(Lyakhovsky et al. 1996) or the ratio of the time scales for diffusion $\sim R^2/D$ and for viscous deformation $\eta/\Delta P$. If the product of $D\eta$ which appears in the denominator of the Pe number does not depend on temperature, the bubble growth time scale τ_{gr} will have an activation energy E_a of diffusion ($Pe>1$, diffusional growth) and E_a of viscous flow ($Pe<1$, expansional growth). If $D\eta$ changes with temperature, it may happen that at some temperature Pe number and the activation energy of the bubble growth timescale will change.

Volume expansion model – Avrami equation. It should be clear at this point that the general expression for the volume expansion integral (1) may be a complicated function of time. Both diffusivity and rheology in-

fluence the kinetics of nucleation and bubble growth, and become incorporated into the integral of the volume expansion. Moreover, the degree of supersaturation during the degassing process also changes with time. Making some assumptions concerning the probability of nucleus formation (dependent on the degree of the supersaturation), the integral (1) can be reduced to a simpler function of time. Assuming that there is a certain number of germ nuclei per unit volume of melt, and that nucleation and diffusional growth occur only in undegassed melt, a more simple analytical expression describing the kinetics of new phase formation can obtained. An example is the Avrami equation for random nucleation and diffusional growth of a new phase (Avrami 1939, 1940) which results in

$$\Delta V_{\mathrm{ph}}(t) \propto \{1 - \exp[-(t/\tau_{\mathrm{av}})^n]\} \quad (3)$$

and predicts sigmoidal curves for the volume fraction $\Delta V_{\mathrm{ph}}(t)$ of the phase separated after time t. The parameter τ_{av} (or characteristic timescale of phase separation) depends both on nucleation and diffusion timescales (characteristic time of phase separation), and n is an exponent having values between 2.5 and 4, depending on the mechanism controlling the phase growth (diffusional or interfacial). The analytical expression of the Avrami equation is easier for practical use than Eq. (1) where induction time τ_{ind} and bubble growth timescale τ_{gr} are two independent parameters. Parameter τ_{av} may be determined experimentally as a function of temperature. The parameter n can be even <2.5 because (a) the bubble growth is expansional and controlled by shear stress relaxation in the melt, and (b) the nucleation is not homogeneous, as some bubbles are already present in the melt before the onset of volume expansion. Knowing the activation energy of τ_{av} and the exponent n, the volume expansion curve can be calculated at any temperature knowing the final volume expansion effect $\Delta V(t=\infty)$. This parameter can be determined from the initial volatile concentration dissolved in the melt and the initial melt volume V_0 using an appropriate equation of state for the separated gas.

Experiment description

We have adopted here a twofold approach to the experimental study of vesiculation processes. Firstly, the direct observation of bubble growth in situ in order to enable the timescale of bubble growth to be established, yielding the parameter $V_{\mathrm{b}}(t)$ of Eq. (1). Additionally, bubble dissolution was observed optically and the effective value of the diffusion rate for water out of dissolving bubbles has been determined. Secondly, changes in volume during vesiculation, $V(t)$ in Eq. (1), were determined using dilatometric measurements.

Sample selection and characterization. The sample studied is a water-bearing, peralkaline rhyolite from the Greater Olkaria Volcanic Complex (GOVC) in the Kenya Rift Valley. The sample has been chosen because of its low glass transition temperature (543 °C) and absence of microlites. The glass is pristine and crystal-poor, with <1 vol.% crystals as determined by optical microscope and SEM inspection. The initial bulk composition is reproduced in Table 1 from Macdonald et al. (1987). The major element chemistry shows a peralkaline composition with an agpaitic index (mol alkali/aluminum) of 1.33. The total water concentration of the sample, determined using a Brucker IFS 120 high-resolution Fourier transform infrared spectrometer, is 0.14 wt.%. This value, mostly OH^- group species, was determined at 3570 cm^{-1} and has been taken as an average of two values 0.16 wt.% (obtained by using the integration of the peak) and 0.12 wt.% (by measuring its amplitude). In calculations we assumed a value of the integrated molar absorptivity of 32000 L/mol cm^2 (Stolper 1982), a value of the molar absorptivity of rhyolitic glass 88 L/mol cm (Dobson et al. 1989), and have determined the density of the rhyolite glass as 2.385 g/cm^3 by Berman balance.

Table 1 Chemical composition of peralkaline rhyolite Olkaria (Kenya)

Oxide	Before experiment[a]	After experiment[b]
SiO_2	73.30	73.8
TiO_2	0.22	0.17
Al_2O_3	10.45	10.0
Fe_2O_3	1.61	—
FeO	2.01	3.9[c]
MnO	0.04	0.07
MgO	0.01	0.01
CaO	0.19	0.09
Na_2O	5.56	5.50
K_2O	4.45	4.20
F	0.62	—
Cl	0.32	—
Total	98.78	97.70

A.I. 1.33 (agpaitic index = Na + K/Al)
[a] From Macdonald et al. 1987
[b] ICP-AES (inductive coupled plasma atomic emission spectrometer). In weight percent using single element solution standards
[c] FeO is taken as a sum of ferric and ferrous iron

Viscosity measurements. The viscosity data at high temperature (1100–1350 °C) have been measured by concentric cylinder viscometry with a Brookfield HBTD (full-scale torque = 0.575 Nm and rotation speeds of 0.5–50 rpm). For these experiments, the natural sample has been remelted at 1650 °C and contained $\approx$0.02–0.03 wt.% H_2O (Keppler and Bagdassarov 1993). The apparatus, technique, and data reduction are described elsewhere (e.g. Dingwell 1989). At low temperatures shear viscosity has been measured by the micropenetration method using a spherical indenter on remelted samples (cylinders 2.5–4 mm in thickness, 8 mm in diameter) in the vertical push-rod dilatometers Netzsch TMA 402 and BÄHR DIL 802V. The method of measurements, calibration technique by using NBS711 glass standards, and the precision of the experiments have been described elsewhere (Dingwell et al. 1992; Hess et al. 1995). In this study water-bearing samples of the peralkaline rhyolite have been measured by this method. The water content before and after micropenetration measurements has been determined by Fourier transform infrared (FTIR) spectroscopy. On each sample the duration of the experiments at different temperatures has been restricted in such a way that changes in absorption spectrum at 3570 cm^{-1} give <0.005 wt.% of water loss as judged from the integration of the absorption peak. The parameters of micropenetration measurements and the results are shown in Fig. 1 and listed in Table 2.

The temperature dependence of shear viscosity follows the Arrhenius relation with the activation energy of viscous flow 71.4 ± 1.8 kcal/mol, $\log(\eta_0) = -5.89 \pm 0.4$ (in Pa s) for the water-free samples and 68.4 ± 1.4 kcal/mol, $\log(\eta_0) = -6.629 \pm 0.011$ (in Pa s) for natural rhyolite samples containing 0.14 wt.% H_2O (see

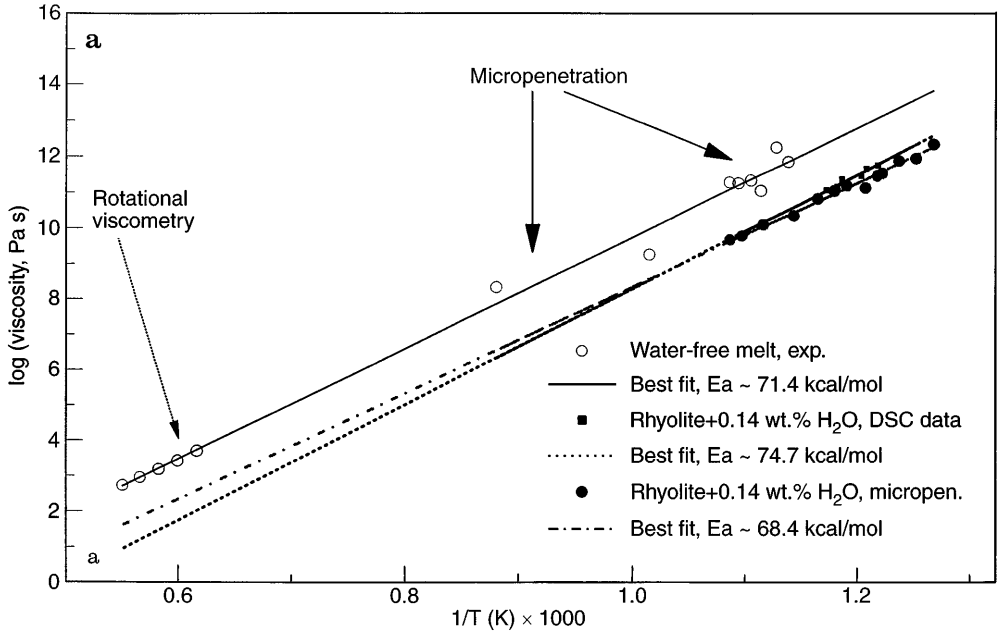

Fig. 1a, b Shear viscosity and the thermal expansion coefficient of the peralkaline rhyolite melt (Olkaria, Kenya). **a** Data on the water-free melt have been obtained by concentric cylinder viscometry (Wilding et al. 1995) and by micropenetration viscometry (Hess, *personal communication*). Viscosity of water-bearing glasses (0.14 wt.% H_2O) have been calculated from differential scanning calorimetry (DSC) (Wilding et al. 1995) and by the micropenetration method (this study). **b** Linear thermal expansion coefficient of peralkaline rhyolite melt as a function of temperature obtained by the dilatometry with the scanning rate 5 °C/min. Temperature 543 °C corresponds to the glass transformation at this heating rate.

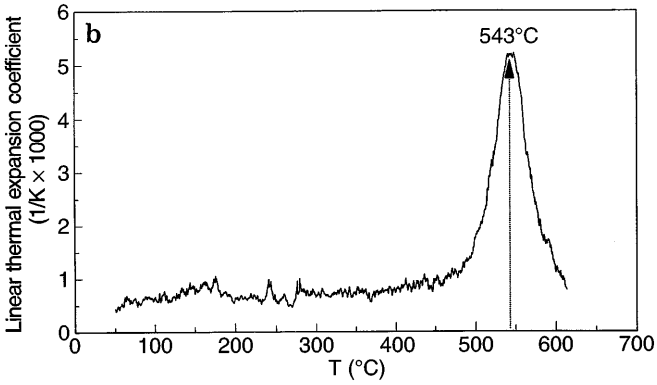

Table 3). From the extrapolation of the micropenetration data to $\log(\eta)=12$ Pa s the rheological glass transition temperature for water free sample is 600 °C and for water-bearing sample 530 °C. The difference of ≈70° is much larger than that calculated by Shaw's (1972) method. The thermal expansion coefficient has been measured as a function of temperature on a natural rhyolite sample (cylindrical sample 15 mm in length, 8 mm in diameter) by using a Netzsch TMA 402 dilatometer with a heating rate of 5 °C/min. The temperature dependence of the thermal expansion coefficient (see the inset in Fig. 1) indicates a peak value near 543 °C in the natural sample, which corresponds to a viscosity ≈11.7 log(Pa s) according to the present shear viscosity measurements.

Optical method. To observe directly the process of bubble growth in this rhyolite melt at high temperature, a heating stage designed by A. Slutsky (Zapunnyy et al. 1989) operating at temperatures up to 1500 °C was used. A cylindrical core of the original rhyolite sample (diameter ~1 mm, length ~1 mm) was mounted in the Pt-foil holder of the heating stage and brought into the focal plane of an optical microscope. During the experiment a stream of Ar passed through the stage in order to protect the Pt-heater and Pt–Rh thermocouple during experiments with a long runtime. The sample was heated at a rate of 400–500 °C/min to 650–900 °C then kept at a fixed temperature controlled to within ±1 °C. The optical observations of the process of bubble growth were recorded by a Sanyo VCC-2972 video camera and stored on a Panasonic AG-6720A-E video recorder with programmed timesteps. The video images of bubbles that were obtained during the run have been stored in the PC and analyzed with the Image Analysis Program (DIAna Bildanalyse). The diameters of growing bubbles (the minimum observable size of bubbles ≈5 μm) were measured on the screen of the PC with a precision of ≈±0.5 μm and the results have been plotted against elapsed time.

Dilatometric method. A laboratory quartz-glass push-rod dilatometer (Model TMA, Netzsch Gerätebau, Selb, Germany) was used in volume expansion measurements (Bagdassarov and Dingwell 1992). Cylindrical samples of natural rhyolite (diameter = 8 mm, L = 3–4 mm) were placed in an alumina crucible (inner diameter 8 mm, outer 10 mm, length 23 mm) lined with Pt-foil. The quartz rod touches the sample via an alumina piston, which can move freely within the crucible and act on the quartz rod. Volume expansion of vesiculated melt was registered by the vertical displacement of the piston–quartz rod–vanadium rod assembly using a calibrated linear voltage displacement transducer (LVDT). The experiments last from several minutes at ~935 °C to 11 days at ~650 °C.

Experimental results

Bubble growth observations. The in situ optical observation of the bubble nucleation process is technically difficult. If the microscope is focused at a particular plane, bubbles that have started to grow in an adjacent area will only be noticed with some delay. Thus, samples for the bubble growth observation were chosen which contained preexisting bubbles. For this purpose the rhyolite sample was cut into slices 8 mm in diameter and 1 mm in thickness. Polished disks were inspected with the optical microscope, and cylinders for heating stage experiments were drilled out from the areas containing bubbles. The initial sizes of bubbles were ~20–50 μm. They have ellipsoidal shape with aspect ratios ~1.2–2.9. The initial minimum distance between bubbles in the sample was more than 200–300 μm. The lin-

Table 2 Shear viscosity of natural peralkaline rhyolite measured by the micropenetration method

T, °C	Log (viscosity; Pa s $\pm 1\sigma$)	Duration of experiment[c] (min)	Diameter of indenter sphere (mm)	Applied load (kg)
515.0[a]	12.41 ± 0.10	150 (120)	1.997	0.85
524.8[a]	12.01 ± 0.08	130 (100)	1.997	0.80
534.6[a]	11.95 ± 0.05	60 (30)	1.997	0.50
544.4[a]	11.60 ± 0.02	40 (20)	1.997	0.50
547.2[b]	11.53 ± 0.01	40 (20)	2.996	0.15
554.4[a]	11.49 ± 0.01	35 (20)	2.996	0.50
566[b]	11.26 ± 0.01	35 (20)	2.996	0.15
573.8[a]	11.09 ± 0.01	30 (15)	2.996	0.25
584.1[a]	10.88 ± 0.01	25 (10)	2.996	0.15
599.9[b]	10.39 ± 0.05	25 (10)	2.996	0.15
621.2[b]	10.12 ± 0.03	20 (5)	3.998	0.15
636.6[b]	9.78 ± 0.03	15 (5)	4.995	0.15
645.6[b]	9.67 ± 0.01	15 (5)	4.995	0.15

[a] Data obtained in the vertical push-rod dilatometer Netzsch TMA 402
[b] Data obtained in the vertical push-rod dilatometer BÄHR DIL 802V. Indenters are alumina spheres (Frialit-Degussit), thickness of glass samples 2.5–4 mm, diameter 8 mm
[c] Duration of the no-load segment is given in parentheses

Table 3 Modeling of shear viscosity of peralkaline rhyolite Olkaria (Kenya)

Composition	Data source, reference	Equation $\mathrm{Log}\,\eta = A + \frac{B}{T, \mathrm{K}}$, Pa s	Activation energy of viscous flow E_a (kcal/mol $\pm 1\sigma$)	Rheological glass transition T_g, °C ($\log \eta \approx 12$ Pa s)
Water-free peralkaline melt, sample remelted at 1650 °C	Rotational viscometry (Wilding et al. 1995) + micropenetration (Hess, *personal communication*)	$-5.89 + \frac{15611}{T, \mathrm{K}}$	71.4 ± 1.8	600
Water-bearing peralkaline rhyolite 0.14 wt.% H_2O	Micropenetration (this study)	$-6.629 + \frac{14957}{T, \mathrm{K}}$	68.4 ± 1.4	530
Water-bearing peralkaline rhyolite 0.14 wt.% H_2O	Calculated from differential scanning calorimetry data (Wilding et al. 1995)	$-8.05 + \frac{16326}{T, \mathrm{K}}$	74.7 ± 6.6	541
Water-free peralkaline melt	Calculated (Shaw 1972)	$-6.19 + \frac{16085}{T, \mathrm{K}}$	73.6	611
Water-bearing peralkaline rhyolite 0.14 wt.% H_2O	Calculated (Shaw 1972)	$-6.15 + \frac{15626}{T, \mathrm{K}}$	72.4	599

Table 4 Parameters of bubble growth experiments

T, °C	Initial D_{max}[a] (μm)	Initial D_{min}[a] (μm)	Log [τ_{lag}; s]	Log [τ_{gr}; s]	Elapsed time when the objective has been changed (s)
650	32	19	4.2	5.75	No change
660	34.5	26	3.7	5.5	No change
675	41	30.5	3.5	5.1	No change
700	35	22.5	2.8	4.72	3×10^4
725	28.5	18	3.2	3.9	2×10^4
730	24.5	20.5	2.7	3.8	2×10^4
735	21.5	10.5	2.4	3.65	1×10^4
765	23	12.5	2.2	3.5	7.2×10^3
770	48	16.5	1.95	3.3	7.2×10^3
775	36	24.5	1.9	3.25	7×10^3
800	31.5	24.5	1.8	3.07	5×10^3
850	29	16.5	1.7	2.5	No change
870	44	39.5	2.2	2.3	3.5×10^2
900	49.5	32.5	1.6	2.15	No change
925	26.5	20.5	1.3	1.97	6×10^2

[a] $D_{max,min}$ the initial maximum and minimum diameters of bubbles
τ_{lag} and τ_{gr} are characteristic timescales of the lag time and bubble growth

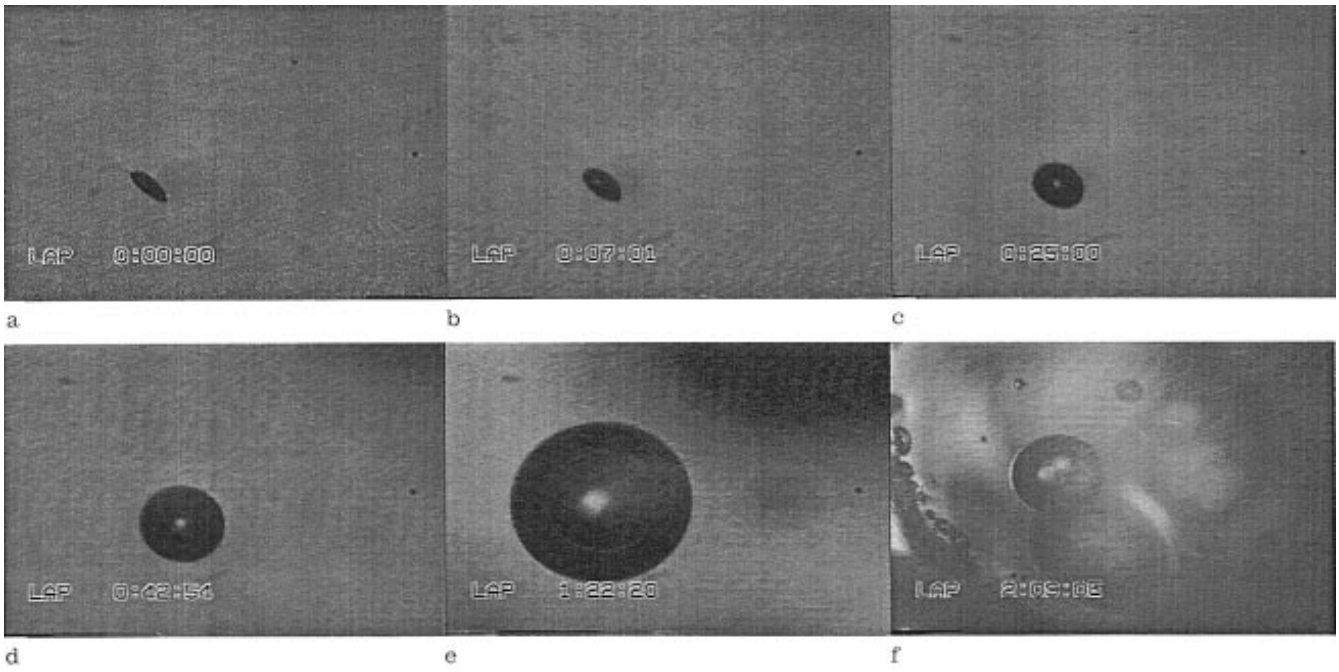

Fig. 2a–f Evolution of bubble growth at 770 °C. **a** bubble initially having a shape of elongated spheroid with a size 48×16.5 μm; **b** 46×25 μm; **c** 56.5×48 μm; **d** 85.5×80 μm; **e** 170 μm; **f** 253.5 μm (the objective has been changed). The indicated elapsed time is in h:min:s

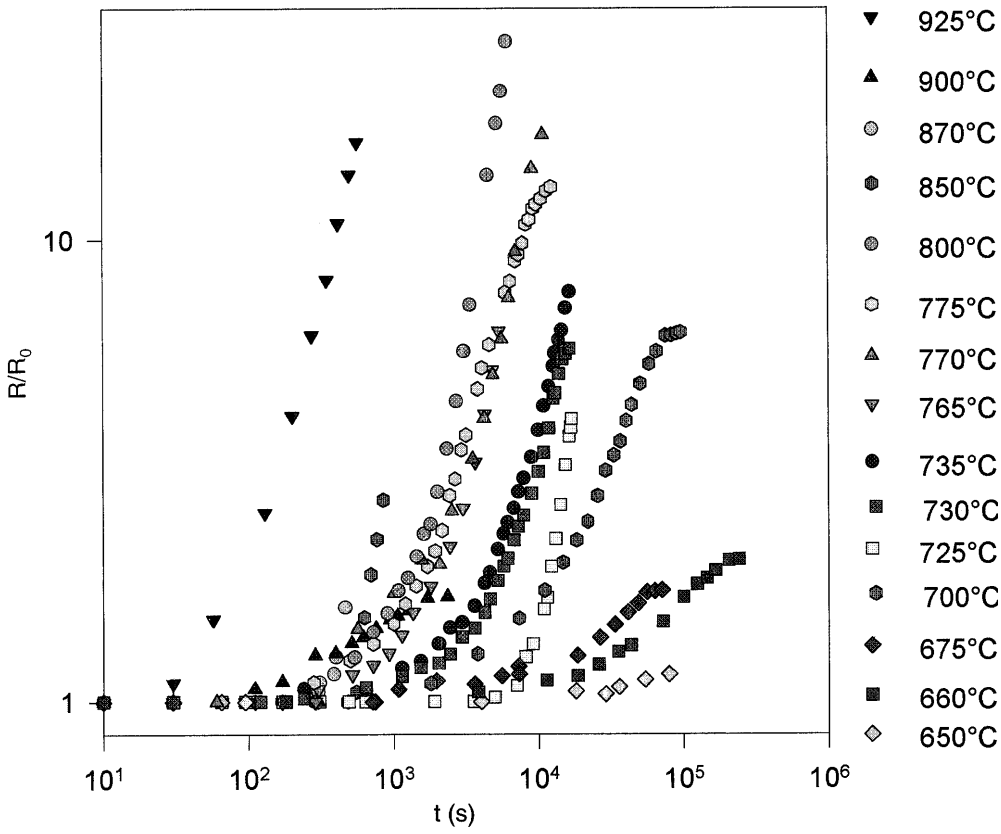

Fig. 3 Bubble growth kinetics in rhyolite melt. R_0 is the initial size of bubbles

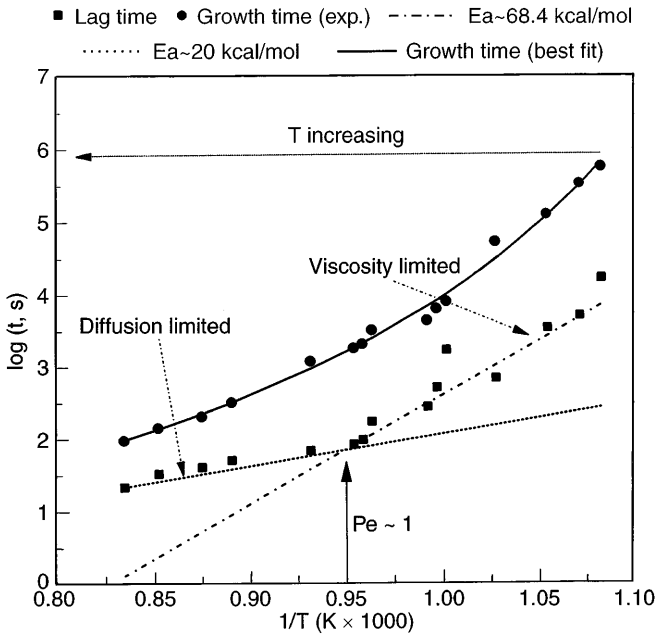

Fig. 4 Lag-timescale of bubble growth. Data on the lag time obtained from Fig. 3 indicate the different activation energies at low and high temperatures. The kink in slope corresponds to the Pe-number $Pe \approx 1$

ear sizes of growing bubbles were recalculated from their volumes $R_b(t) = [3V_b(t)/4\pi]^{1/3}$ where $V_b(t)$ was calculated from measured diameters. The conditions of the experiments and initial sizes of growing bubbles are indicated in Table 4. When bubbles reached a size >200–300 μm, the objective was changed to a lower magnification.

The typical evolution of bubble growth is shown in Fig. 2. At all temperatures bubbles start to grow only after a certain time lag (Fig. 3). This time lag has been estimated as the time at which the volume of the bubble increases by 5%. This lag time between the attainment of the run temperature and the detection of bubble growth is an Arrhenian function of temperature

$$\tau_{lag}(T) \sim \tau_0 \exp(-E_a/RT), \tag{4}$$

where τ_0 is a fitting parameter, and R is the gas constant (Fig. 4). The calculated activation energy E_a of the lag time at $T > 790$ °C is ~68.4 kcal/mol, which is equal to the activation energy of viscous flow of the rhyolite melt obtained from the micropenetration measurements. The kink in slope of $\log[\tau_{lag}]$ vs $1/T$,K corresponds to the temperature 790 °C (Fig. 4). At the temperature 750 °C the Pe-number calculated by using viscosity data (Table 2) and the bulk water diffusion coefficient (Jambon et al. 1992) is ≈1 for bubbles with radius 15 μm and $\Delta P = 1$ bar. At lower temperatures, $Pe \ll 1$, at higher temperatures $Pe \gg 1$. The lag time of bubble growth in viscous melts observed here may be controlled by the timescale of nuclei shape relaxation. In that case we may interpret the observed time-lag as the shape relaxation time τ_{shape} of nonspherical bubbles

$$\tau_{shape} \sim \eta R/2\sigma, \tag{5}$$

where R is the minimum curvature radius of the bubble shape and σ is the surface tension of the melt (Schowalter 1978). This expression can be written by analogy with the Maxwell relaxation time assuming that a vesicle has the effective rigidity $\sim 2\sigma/R$. The calculations show that for a bubble with the radius of curvature $R = 5$ μm and $\sigma = 0.25$ N/m, $\log[\tau_{shape}, \text{s}] \approx 3.36$ at 725 °C and ≈4.57 at 650 °C which correspond to observed lag times of 3.2 and 4.2, respectively (see Table 4). At high temperatures the timescale of bubble growth has a smaller slope as a function of temperature. The slope is close to the activation energy of molecular water diffusion in rhyolite melt ~20 kcal/mol (e.g., Zhang et al. 1991). The *Pe*-number of these bubbles is ≫1. Thus, the lag time of bubble growth can be approximated as

$$\log[\tau_{lag}] = -12.36 + \frac{14950}{T, \text{K}} \quad (650\,^\circ\text{C} < T < 790\,^\circ\text{C}) \tag{6}$$

and

$$\log[\tau_{lag}] = -2.32 + \frac{4371}{T, \text{K}} \quad (790\,^\circ\text{C} < T < 925\,^\circ\text{C}). \tag{7}$$

Another method of modeling the data is to fit the growth curve to the exponential relation

$$\ln\left(\frac{R}{R_0}\right) = \frac{t - \tau_{lag}}{\tau_{gr}}, \tag{8}$$

at $t > \tau_{gr}$. The fitting parameters of Eq. (8) are shown in Fig. 4 and in Table 3. The temperature dependence of τ_{gr} is significantly non-Arrhenian

$$\log[\tau_{gr}] = -0.744 + \frac{1284.6}{T, \text{K} - 726.8}. \tag{9}$$

The slope of $\log[\tau_{gr}]$ vs $1/T$ tends asymptotically to the activation energy of viscous flow at $T < 790$ °C and to the activation energy of diffusion coefficient at $T > 790$ °C.

The experimental data on bubble growth have been compared with the calculated growth by using the ARCO program for solving the equations governing the diffusional growth of a bubble in a Newtonian fluid (Arefmanesh et al. 1990) with the modifications for the water solubility in the rhyolite melt $C_{H_2O} = K_h\sqrt{P}$. The initial uniform water concentration in the melt has been taken as 0.14 wt.%, the solubility at 1 bar is 0.1 wt.%, the viscosity of rhyolite melt is from this study, the bulk water diffusion coefficient is from Jambon et al. (1992), the initial radius of a bubble is 15 μm, and the initial distance between bubbles is 300 μm. The results of calculations and experiments are shown in Fig. 5. The dif-

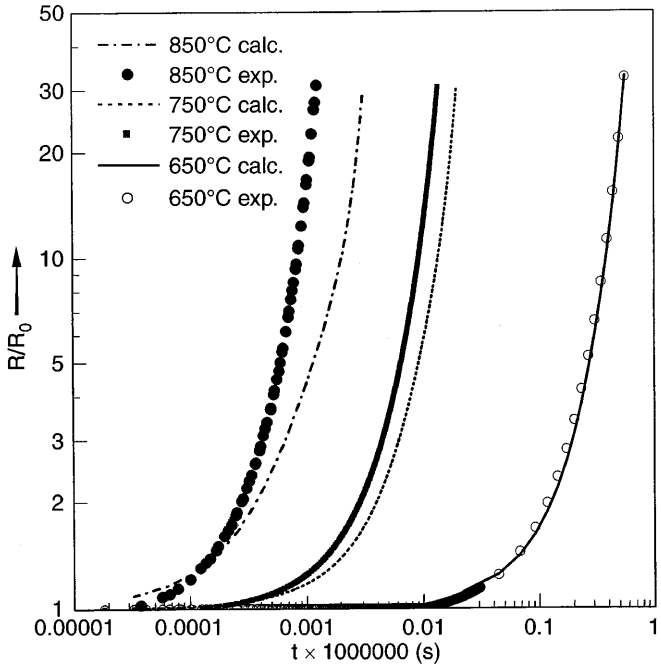

Fig. 5 Comparison of the calculated bubble size R/R_0 with experimental results. With the increasing temperature a systematic deviation of the experimental bubble growth data from the calculated one is observed

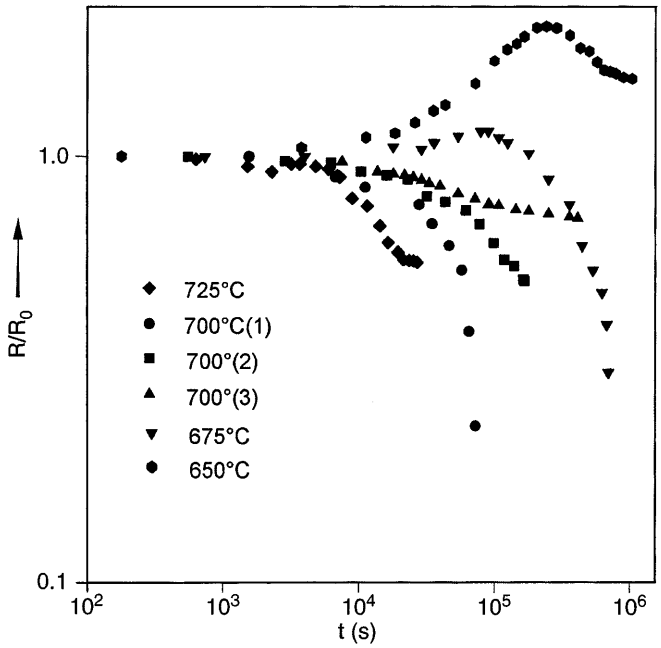

Fig. 6 Bubble dissolution experiments. R_0 is the initial size of bubbles. 700 °C (*1*): dissolution in a nonannealed sample; 700 °C (*2*): in a sample annealed at 900 °C for 40 min; 700 °C (*3*): in a sample annealed at 900 °C for 1 min

ference in the observed and calculated bubble growth can be attributed to the nonuniform H_2O concentrational profile around the bubble and uncertainties in the equilibrium solubility of water as a function of temperature.

In other experiments the bubble dissolution process has been studied. Bubbles formed by annealing of samples at high temperature ($\sim$900 °C) were subsequently annealed at lower temperatures, and their dissolution rates have been measured (Fig. 6). The reason for the bubble dissolution lies in the temperature dependence of water solubility in rhyolite melt at low pressures (Holz et al. 1995). The vapor in bubbles, for which the dissolution has been observed (nucleated at high temperatures and then annealed at lower temperatures) partially dissolves back in the melt resulting in their size decrease.

Dilatometric results. A typical temperature–volume curve (Fig. 7) of volume expansion consists of three temperature segments. The first corresponds to the vesiculation regime of the water-bearing melt. The second segment reflects a steady-state volume of foam and corresponds to the coalescence of bubbles in the melt. The third and final stage is a decrease of the foam volume and corresponds to the bursting of bubbles near the sample surface.

All the expansion curves at different temperatures are similar in shape (Fig. 8) and differ only in characteristic timescale. The incubation period is the time required after the establishment of constant temperature and supersaturation for the appearance of detectable increase of volume (5%) and includes the process of embryo generation (nucleation) and growth to a detectable size. The volume–time curves obtained at different temperatures have been fitted to the Avrami equation (3). The decay stage of foams has been fitted to the exponent with the characteristic time of bubble loss. The example of the fit and different stages of the volume expansion are shown in Fig. 7. The temperature dependence of three characteristic timescales – induction–incubation, volume expansion according to the Avrami equation, and bubble loss – are close to Arrhenian (Fig. 9). The temperature dependence of the induction time has an activation energy $\approx 73.4 \pm 4.5$ kcal/mol, close to that of viscous flow of 68.4 kcal/mol. The fit of the data to the Avrami growth rate (Eq. (3)) with $n \approx 2.5$ (excluding the incubation stage) shows a slightly smaller activation energy (48.5 ± 3.5 kcal/mol) for this characteristic timescale, τ_{av}, but one which is still close to the activation energy of viscous flow.

The bubble loss stage consists of the period from the steady state of foam volume to the completion of bubble bursting through the surface of the sample. The characteristic time of this process has the activation energy of $E_a \sim 47.4$ kcal/mol (Fig. 9). In general, bubble loss at constant foam volume has two sources: (a) coalescence due to rupture of bubble walls and (b) ripening due to gas diffusion from small bubbles to larger bubbles (Lemlich 1972). At a later stage bubbles escape at the surface of the sample resulting in a volume decrease. This includes: (a) liquid (melt) drainage in the "Plateau borders" and films between bubbles and the outer boundary of the sample (e.g. Bikerman 1973;

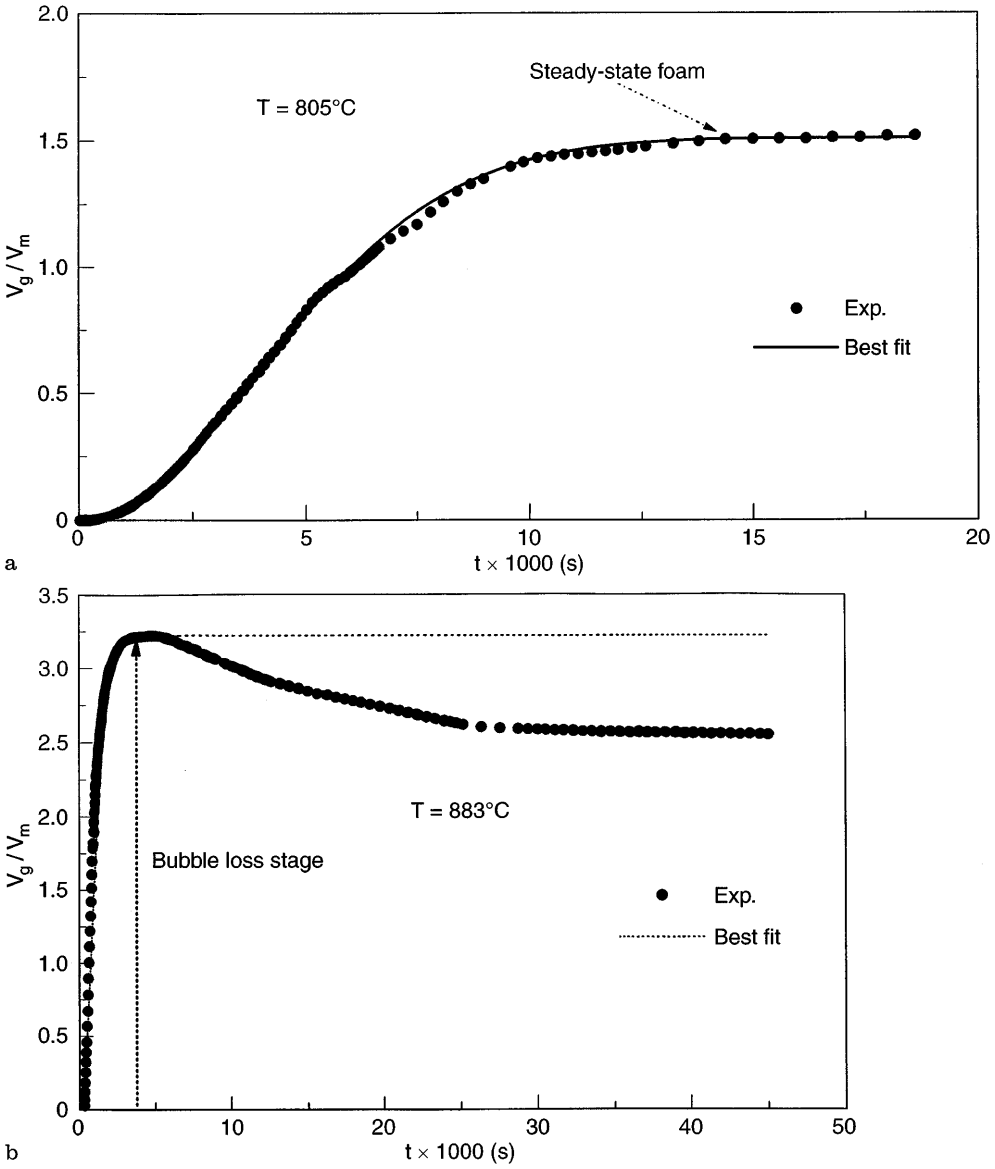

Fig. 7a, b The kinetic data obtained for rhyolite melt expansion. **a** Volume expansion data obtained between the starting point of vesiculation and the steady state of foam are fitted to the Avrami equation (3). **b** Volume decrease data during the foam collapse stage have been fitted to the exponent $\propto \exp(-t/\tau_{col})$

Kraynik 1988); (b) gas diffusion through liquid films comprising the surface of the sample (Lemlich 1972); and (c) mechanical rupture of these films (de Vries 1972). The time dependence of mechanical rupturing of bubbles bursting at the free surface of the melt is also scaled by shear viscosity (Boulton-Stone and Blake 1993). The estimation of a bubble loss time can be done by using Eq. (5). For bubble size 150 μm, surface tension 0.25 N/m and shear viscosity obtained in this study, $\log[\tau_{col}, s]$ of bubble loss is 6.05 at 650 °C and 4.46 at 750 °C. The estimated $\log[\tau_{col}, s]$ in Fig. 9 are 5.9 and 4.62, respectively. At higher temperatures (~950 °C) the observed bubble loss time is larger than the calculated bubble loss time by ≈1.4 log unit. The melt drainage process according to Eq. (5) should have an activation energy of shear viscosity (68.4 kcal/mol). The observed bubble loss process has smaller activation energy (47.4 kcal/mol). At the same time the water diffusion process in rhyolite melt has an activation energy ≈11 kcal/mol (Jambon et al. 1992). Thus, the joint effect of mechanical bubble loss at the free surface and gas diffusion through films of surface bubbles into the external space may yield an intermediate value of activation energy and slow the process of bubble loss.

The exponent n in the Avrami equation (3) varies slightly with temperature (Fig. 10). At temperatures close to T_g (650–700 °C) $n \sim 2.5$. At higher temperatures nucleation and growth have significantly distinct timescales and the superposition of two processes in Eq. (1) would probably contribute to the integral effect of volume expansion giving exponent $n < 2.5$. Another reason for the exponent being smaller than 2.5 is that some bubbles did not nucleate; insteads they expanded without a nucleation time lag.

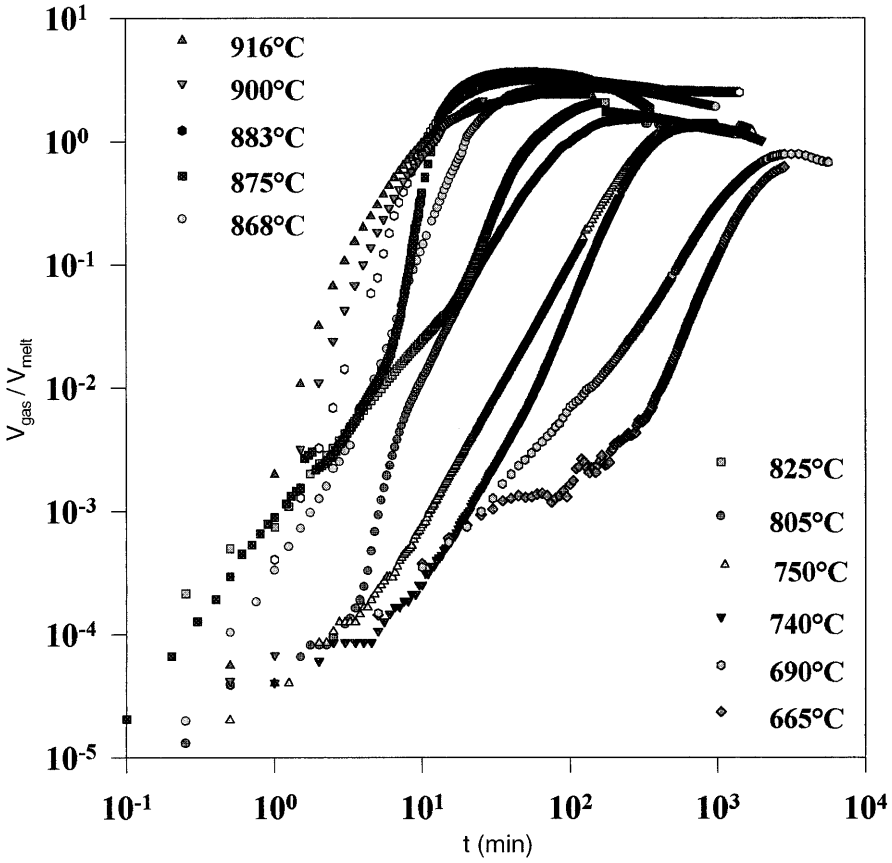

Fig. 8 Volume expansion data obtained by the dilatometry for peralkaline rhyolite melt at different temperatures

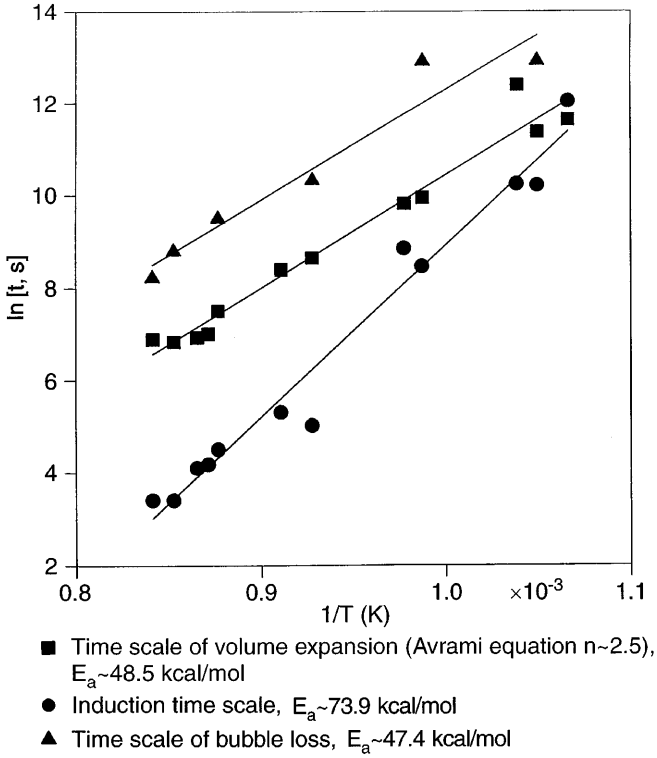

Fig. 9 The characteristic timescales of vesiculation processes in peralkaline rhyolite melt. The best fit of data: induction time $\ln[\tau_{ind}, s] = -28.76 + 37184/T, K$; characteristic time of the Avrami equation (3) $\ln[\tau_{av}, s] = -13.93 + 24375/T, K$; bubble loss or foam collapse time $\ln[\tau_{col}, s] = -11.56 + 23859/T, K$

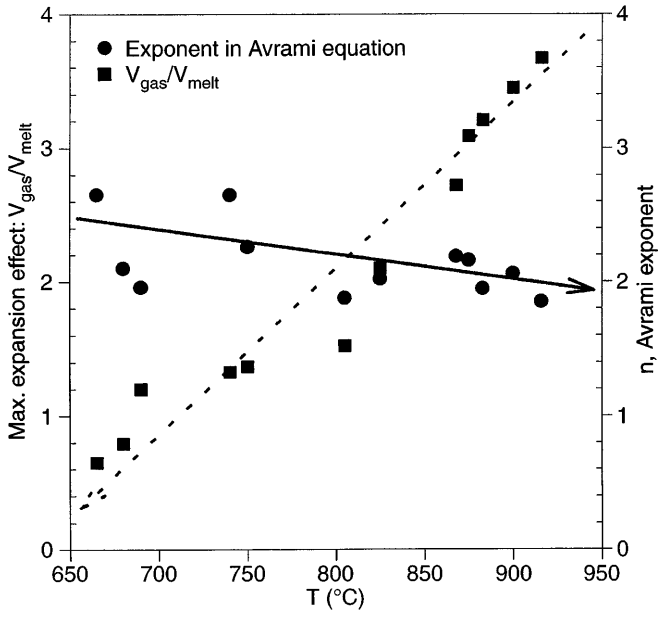

Fig. 10 Temperature dependence of the maximum expansion effect of foaming V_g/V_{melt} and the exponent n in the Avrami equation in peralkaline rhyolite melt

Discussion

Domes or dome-like structures formed by the extrusion of viscous lavas of felsic composition varying from rhyolite to andesite are natural objects where the process of phase separation between vapor and melt occurs. These volcanic edifices represent sites of slow vesiculation and volume expansion of silicic magma. The initial shape of some of these features is hemispheric, with the expanded viscous magma sometimes pushing up the surrounding host rocks to form so-called cryptodomes (c.f. Tazieff 1982). The growth of silicic domes or dome complexes is commonly associated with the passive release of gases at depth from a rising mass of viscous lava (Fink et al. 1992). The viscosity of dome lavas is high (10^5–10^{12} Pa s; Murase and McBirney 1973) and the extrusion process may continue over several months or years (Wohletz and Heiken 1992). Silicic lava textures (volatile-rich pumices, coarsely pumiceous rhyolite lavas, glassy obsidians, finely pumiceous lavas, and crystalline rhyolites) possess distinct rheologies varying from that of a viscous Newtonian to a visco-plastic Bingham fluid (Fink 1980). Depending on the strain rate, vesicular melt can exhibit higher or lower viscosity than bubble-free melt (Bagdassarov and Dingwell 1992, 1993). The present analysis of bubble growth in viscous media may be applicable to the prediction of silicic dome mechanical behavior and evolution (Eqs. (1) or (3)).

The common textural arrangement in these silicic domes involves layering of obsidian with coarsely and finely vesiculated pumices (Fink 1983). These textures result from the combined effects of cooling and vesiculation, flow stresses in the core of the dome, and quenching of carapace or the upper surface (Fink and Manley 1987). The carapace of a silicic dome represents relatively cool and stronger material than the core. Being on the surface and exhibiting a more elastic behavior with higher yield strength than magma within the dome center, the carapace fractures when subjected to rapidly-applied stress or to thermal contraction (c.f. Walker 1969). The hardness and effective strength of the carapace at high strain rates combined with viscous behavior at lower strain rates provide steady growth resulting from slow volume expansion due to volatile separation (slow internal stresses). At the same time, disruption or fracturing of the carapace may result in propagation of depressurization waves (fronts of weak discontinuity) toward the core of the dome (Fink and Manley 1987; Fink and Kieffer 1993). Thus, the slow and delayed vesiculation in viscous silicic magmas followed by the fast release of pressure within the core of volcanic domes are among the most important factors determining the kinetics of pyroclastic activity. The unloading wave or fast release of external stresses may result from the gravitational collapse of domes sometimes causing, for example, pyroclastic flows of *Merapi* and *Peleean* types (Williams and McBirney 1979).

The triggering mechanism for Merapi type flows may be either a landslide of the volcanic edifice, earthquakes, or thermal cracking of the carapace. The main feature of these flows is that they are not of explosive volcanic origin. The ease of disaggregation of vesicular material forming the dome center has already been facilitated by the long and slow degassing process of slightly supersaturated and very viscous magma. The significant induction time for bubble nucleation or delay between the stage of supersaturation and starting of volume expansion in silicic magmas means that this type of eruption will be governed by a stochastic process (Shimozuru 1991). The front of a disaggregation wave which is generated locally by the release of pressure in a vesicular magma may also sporadically decay when it reaches a level where the porosity of magma is low enough due to the delayed vesiculation. The mechanism of this bursting wave initiation and damping has been theoretically considered for the case of gas-bearing porous rocks (e.g. Nikolsky 1953).

Peleean type flows are more destructive, and take place at an early stage of silicic dome growth. These types of explosions are commonly laterally directed. They are triggered by the weakening and fracturing of surrounding rocks caused by the stresses associated with dome growth (Heiken and Wohletz 1991). Stress growth in surrounding rocks may also be due to slow degassing and volume expansion of magmas, but the scale of stresses may be significantly larger owing to a higher stiffness of the host rock.

Possible increases in explosive activity with time during the emplacement of silicic lavas is supported by observations of volcanic craters on the surface of some rhyolite flows (Fink and Manley 1989). These secondary explosions which have been delayed due to slow volatile separation from silicic magmas make the advancing lava flow a potential source of pyroclastic flows. The time delay or distance from the vent where these explosions can start may be predicted using the Avrami expression knowing magma temperature, viscosity, composition, and volatile content. If the rate of lava flow advance is greater than the volume expansion rate at a given temperature, the probability of secondary explosions is small. If the rate of lava flow is much smaller than the expansion rate of the gas-melt mixture according to Eq. (3), then the flow surface can generate explosive pits and the flow front can collapse leading to generation of pyroclastic flows. The maximum expansion rate according to Eq. (3) occurs at $t \approx \tau_{av}$. Thus, the minimum distance from the vent at which secondary explosions may occur can be estimated as

$$L \approx \frac{\rho h^2 g \sin\alpha}{3\eta}\,\tau_{av}, \tag{10}$$

where h is a thickness, α is a slope, and ρ is the density of the flow. At $T = 630\,^{\circ}\mathrm{C}$ according to this study $\tau_{av} = 10^6$ s, $\eta = 10^{10}$ Pa s. Assuming $\alpha = 20^{\circ}$, $\rho = 2.4$ g/cm^3, and the thickness of flow $h \approx 85$ m, the distance L

calculated from Eq. (10) is ≈ 2 km. At approximately this distance the collapse of the over-steepened front of the El Brujo dacite flow (Santiago Volcano, Guatemala) has been observed (Fink and Manley 1989).

For the prediction of silicic dome behavior and evolution, the present analysis of bubble nucleation and growth in viscous media may be applicable (Eqs. (1) or (3)). Field data on the cryptodome growth of Mount St. Helens (Swanson and Holcomb 1990) indicate the episodic character of the dome growth against time. Thus, it may be that the endogenous growth of the dacite dome of the Mount St. Helens consisted of a number of discrete magmatic episodes caused by the input of a new portion of magma from below. If the endogenous dome growth assumed to be due to degassing and vesiculation of the dacitic magma, the kinetics of the volume expansion during each of episodes must obey the Avrami relationship. Unfortunately, there is not enough observation of each endogenous growth episode in order to check the applicability of the Avrami equation. According to the field observations, the dome growth represents a sequence of extrusion episodes preceded by periods of endogenous growth which accelerated almost exponentially to the time of the extrusion. The moment of endogenous growth acceleration may correspond to the inflection point on the Avrami curve of volume expansion (Eq. (3). If this assumption is true, duration of each endogenous growth (1–3 weeks) has to correspond to the Avrami characteristic time of volume growth $\tau_{av} \approx 6\text{–}18 \times 10^5$ s; the volume of each extrusion relates to $\Delta V \approx 1.2\text{–}22.4 \times 10^6$ m^3 in Eq. (3). Assuming that the maximum porosity of degassed magma is $\varphi \approx 75$ vol%, the input volume of fresh magma can be estimated as $\Delta V_m \approx \Delta V(1-\varphi)/\varphi = 0.4 - 7.5 \times 10^6$ m^3. The cumulative volume of magma extrusion (integral effect of each eruptive episode) of the Mount St. Helens dome can either be interpreted as having three straight line segments (Swanson and Holcomb 1990) or having a single power law functional relationship (Fink et al. 1990).

From our determination of the kinetics of bubble growth we show that at temperatures close to the glass transition temperature, T_g the temperature dependence of the characteristic timescales of new phase nucleation and growth have activation energies comparable to those for shear relaxation (viscous flow). This means that for cooling felsic magmas, volatiles diffuse into bubbles at a rate which decreases more slowly than the shear viscosity will increase. Comparing activation energies of the diffusion coefficient we find that for molecular water the activation energy is 20 kcal/mol, for bulk water diffusion it is ~ 11 kcal/mol (Jambon et al. 1992), for water interconversion it is even smaller (8.6 kcal/mol, e.g. Dingwell and Webb 1990; Romano et al. 1995), but for viscous flow of rhyolite melts it is 68.4 kcal/mol for peralkaline rhyolite (this study), and can be up to 102 kcal/mol for calc-alkaline rhyolite (Stevenson et al. 1995). Thus, as temperature decreases shear stresses near a growing bubble relax more slowly than the diffusion of volatile species, i.e., viscosity becomes too high relative to diffusion to allow the further bubble growth. Consequently, cooling of vapor bubbles results in a freezing of their size because their contraction is hindered by slow viscous relaxation (Cable and Frade 1994; Romano et al. 1994). Very slow cooling at high temperatures may affect the dissolution of small bubbles before the effect of viscosity is observed. Gas pressure in vesicles formed at high temperature and cooled to temperatures close to T_g will decrease because the contraction of a gas bubble is significantly slowed due to the viscosity increase. This effect relates to the trapping temperature of fluid inclusions in silicate melts (Romano et al. 1994). By holding temperature near the glass transition, the gas pressure slowly recovers due to continuing gas diffusion into vesicles. The final pressure in vesicles may slightly exceed that in the surrounding liquid, but only because of surface tension effects. The cooling rate at which size "freezing" can be observed depends on the ratio between the characteristic time of bubble growth τ_{gr} (contraction in this case) and the characteristic time of gas contraction

$$\tau_{gas} = \left[\alpha_{gas} \frac{dT}{dt} \right]^{-1}, \quad (11)$$

where α_{gas} is the thermal expansion coefficient of gas. The bubble size "freezing" effect in magmas occurs when $\tau_{gr} \gg \tau_{gas}$.

Thus, for magmas containing dissolved volatiles the volcanological importance of the temperature interval in which *Pe*-number ≈ 1 in this context is the crossover point between the gas-diffusion-controlled vapor phase growth and high-viscosity-controlled expansional growth. Finally, significant overpressure of bubbles in vesicular magmas can be achieved only by the decompression of vesicular melts at temperatures close to or below T_g, when *Pe*-number $\ll 1$. This overpressure may be attributed to the expansion of gas (due to the ambient pressure release) providing slow viscous relaxation in the melt.

Conclusions

1. Experimental results on the time-lag between the moment of supersaturation and the beginning of the vesiculation process indicate that a critical cooling rate of magmatic systems is needed in order for water-bearing melts to start to vesiculate. Magmas for which the characteristic time of cooling on the surface is less than the induction time of vesiculation *do not foam*; insteads they retain their initial water content.
2. The timescale of the shear stress relaxation constrains the timescale of nucleation, bubble growth, and bubble loss processes in highly viscous silicic magmas ($Pe \ll 1$).

3. The rate of volume expansion during this process is determined by the Avrami equation with exponent close to 2–2.5. In this equation the activation energy of the temperature dependence of τ_{av} can be taken to be the same as the activation energy of viscous flow.

Acknowledgements We thank H. Schulze and R. Weigel for technical help, Dr. H. Keppler and Dr. C. Romano for the assistance in obtaining IR-spectra, K.-U. Hess for the assistance in micropenetration measurements, A.-M. Dietel for the ICP analysis, Dr. A. Slutzky (Vernadsky Institute, Moscow) for providing a heating stage, Dr. V. Solomatov (Caltech, Pasadena), Dr. R. Stevenson and Dr. J. Mungall for discussions, Prof. S. Advani (Delaware) for the computer code ARCO, Prof. O. Navon and his colleagues for a manuscript of their paper, and Dr. C. Manley (Tempe, Arizona) for useful references. Critical reviews of Prof. J. Fink, Prof. Y. Zhang, and Dr. M. Mangan improved the manuscript significantly. This research was supported by the "Deutsche Forschungsgemeinschaft Gerhard-Hess-Programm" (Di 431/3-1 to DBD).

References

Arefmanesh A, Advani SG (1991) Diffusion-induced growth of a gas bubble in a viscoelastic fluid. Rheol Acta 30:274–273

Arefmanesh A, Advani SG, Michaelidis EE (1990) A numerical study of bubble growth during low pressure structural foam molding process. Polymer Eng Sci 30 (20):1330–1337

Avrami M (1939) Kinetics of phase change. I. General theory. J Chem Phys 7:1103–1112

Avrami M (1940) Kinetics of phase transition II. Transformation time relations. J Chem Phys 8:212–224

Bagdassarov NS, Dingwell DB (1992) A rheological investigation of vesicular rhyolite. J Volcanol Geotherm Res 50:307–322

Bagdassarov NS, Dingwell DB (1993) Deformation of foamed rhyolites under internal and external stresses: an experimental investigation. Bull Volcanol 55:147–154

Bikerman JJ (1973) Foams. Springer, Berlin Heidelberg New York, pp 1–337

Bottinga Y, Javoy M (1991) The degassing of Hawaiian tholeiite. Bull Volcanol 53:73–85

Boulton-Stone JM, Blake JR (1993) Gas bubbles bursting at a free surface. J Fluid Mech 254:437–466

Burn I, Roberts JP (1970) Influence of hydroxyl content on the diffusion of water in silica glass. Phys Chem Glasses 11:107–114

Cable M, Frade JR (1994) The effect of viscosity on the behavior of bubbles in viscous liquids. Phys Chem Glass 35:231–238

Dingwell DB (1989) Shear viscosities of ferro silicate liquids. Am Mineral 74:1038–1044

Dingwell DB, Webb SL (1990) Relaxation in silicate melts. Eur J Mineral 2:427–449

Dingwell DB, Knoche R, Webb SL (1992) The effect of B_2O_3 on the viscosity of haplogranitic liquids. Am Mineral 77:457–461

Dobson PF, Epstein S, Stolper E (1989) Hydrogen isotope fractionation between coexisting vapor and silicate glasses and melts at low pressure. Geochim Cosmochim Acta 53:2723–2730

Fink JH (1980) Surface folding and viscosity of rhyolite flow. Geology 8:250–254

Fink JH (1983) Structure and emplacement of a rhyolitic obsidian flows: Little Glass Mountain, Medicine Lake Highland, northern California. Geol Soc Am Bull 94:362–380

Fink JH (1992) Mount Unzen rumbles on. Nature 357:119

Fink JH, Kieffer SW (1993) Estimate of pyroclastic flow velocities resulting from explosive decompression of lava domes. Nature 363:612–615

Fink JH, Manley CR (1987) Origin of pumicious and glassy textures in rhyolite flows and domes. Geol Soc Am Spec Publ 212:77–88

Fink JH, Manley CR (1989) Explosive volcanic activity generated from within advancing silicic lava flows. IAVCEI Proc Volcanol 1:169–179

Fink JH, Malin MC, Anderson SW (1990) Intrusive and extrusive growth of the Mount St. Helens lava dome. Nature 348:435–437

Fink JH, Anderson SW, Manley CR (1992) Textural constrains on effusive silicic volcanism: beyond the permeable foam model. J Geophys Res 97:1135–1141

Fisher RV, Schmincke H-U (1984) Pyroclastic rocks. Springer, Berlin Heidelberg New York, pp 1–474

Heiken G, Wohletz K (1991) Fragmentation processes in explosive volcanic eruptions. In: Sedimentation in volcanic settings, Society for Sedimentary Geology, Spec Publ 45, pp 19–26

Hess K-U, Dingwell DB, Webb SL (1995) The influence of excess of alkalis on the viscosity of a haplogranitic melt. Am Mineral 80:297–304

Holz F, Behrens H, Dingwell DB, Johannes W (1995) H_2O solubility in haplogranitic melts: compositional, pressure, and temperature dependence. Am Mineral 80:94–108

Hurwitz S, Navon O (1994) Bubble nucleation in rhyolite melts: experiments at high pressure, temperature, and water content. Earth Planet Sci Lett 122:267–280

Jambon A, Zhang Y, Stolper EM (1992) Experimental dehydration of natural obsidian and estimation of D_{H_2O} at low water contents. Geochim Cosmochim Acta 56:2931–2935

Kashchiev D (1969) Solution of the non-steady state problem in nucleation kinetics. Surf Sci 14:209–220

Keppler H, Bagdassarov N (1993) High-temperature FTIR spectra of H_2O in rhyolite melt to 1300 °C. Am Mineral 78:1324–1327

Kirkpatrick RJ (1976) Towards a kinetic model for the crystallization of magma bodies. J Geophys Res 81:2565–2571

Kraynik AM (1988) Foam flows. Annu Rev Fluid Mech 20:325–357

Lemlich R (1972) Principles of foam fractionation and drainage. In: Lemlich R (ed) Adsorptive bubble separation techniques. Academic Press, New York, London, pp 33–51

Lemlich R (1978) Prediction of changes in bubble size distribution due to interbubble gas diffusion in foam. Ind Eng Chem Fundam 17:89–93

Lyakhovsky V, Hurwitz S, Navon O (1996) Bubble growth in rhyolitic melts: experimental and numerical investigation. Earth Planet Sci Lett (in press)

Macdonald R, Davies GR, Bliss CM, Leat PT, Bailey DK, Smith RL (1987) Geochemistry of high-silica peralkaline rhyolites, Naivasha, Kenya Rift Valley. J Petrol 28:979–1008

Mangan MT, Cashman KV, Newman S (1993) Vesiculation of basaltic magma during eruption. Geology 21:157–160

Murase T, McBirney A (1973) Properties of some common igneous rocks and their melts at high temperatures. Geol Soc Am Bull 84:3536–3592

Nikolsky AA (1953) Bursting waves in gas-bearing rocks. Dokl AN SSSR 88:623–626 (in Russian)

Proussevitch AA Sahagian DL, Anderson AT (1993) Dynamics of diffusive bubble growth in magmas: Isothermal case. J Geophys Res 98 22,283–22,307

Romano C, Dingwell DB, Sterner SM (1994) Kinetics of quenching of hydrous feldspatic melts: quantification using synthetic fluid inclusions. Am Mineral 79:1125–1134

Romano C, Dingwell DB, Behrens H (1995) The temperature dependence of the speciation of water in $NaAlSi_3O_8$-$KAlSi_3O_8$ melts: an application of fictive temperature derived from synthetic fluid-inclusions. Contrib Mineral Petrol 122:1–10

Sahagian DL, Proussevitch AA, Anderson AT (1994) Reply to Sparks. J Geophys Res 99 17,829–17,833

Schowalter WR (1978) Mechanics of non-Newtonian fluids. Pergamon Press, Oxford, pp 1–300

Scriven LI (1959) On the dynamics of phase growth. Chem Eng Sci 10:1–13
Shaw HR (1972) Viscosities of magmatic silicate liquids. Am J Sci 272:870–893
Shimozuru D (1991) In the volcano's shadow. Nature 353:295–296
Sparks RSJ (1978) The thermodynamics of bubble formation and growth in magmas: a review and analysis. J Volcanol Geotherm Res 3:1–37
Sparks RSJ (1994) Comment on "Dynamics of diffusive bubble growth in magmas: Isothermal case" by AA Proussevitch, DL Sahagian, and AT Anderson. J Geophys Res 99 17,827–17,828
Sparks RSJ, Barclay J, Jaupart C, Mader HM, Phillips JC (1994) Physical aspects of magmatic degassing. I. Experimental and theoretical constraints on vesiculation. In: Carroll MR, Holloway JR (eds) Review in mineralogy 30, Mineral Soc Am, pp 413–444
Stevenson RJ, Dingwell DB, Webb SL, Bagdassarov NS (1995) The equivalence of enthalpy and shear stress relaxation in obsidians and quantification of the liquid-glass transition in volcanic processes. J Volcanol Geophys Res 68:297–306
Stolper E (1982) Water in silicate glasses: an infrared spectroscopic study. Contrib Mineral Petrol 81:1–17
Swanson DA, Holcomb (1990) Regularities in growth of the Mount St. Helens Dacite Dome, 1980–1986. In: Fink J (ed) Lava flows and domes. Springer, Berlin Heidelberg New York, pp 6–24
Tazieff H (1982) Domes de magma et domes de laves. C R Acad Sci Paris, Series II, 294:151–153
Thomas R (1994) Estimation of the viscosity and the water content of silicate melts from melt inclusion data. Eur J Mineral 6:511–535
Toramaru A (1989) Vesiculation process and bubble size distributions in ascending magmas with constant velocities. J Geophys Res 94 17,523–17,542
Toschev S (1973) Homogeneous nucleation. In: Hartman P (ed) Crystal growth: an introduction. Elsevier, New York, pp 1–49
Vries de A (1972) Morphology, coalescence, and size distribution of foam bubbles. In: Lemlich R (ed) Adsorptive bubble separation techniques. Academic Press, New York, London, pp 7–31
Walker GPL (1969) The breaking of magma. Geol Mag 106:166–173
Wilding MC, Webb SL, Dingwell DB (1995) Evaluation of a relaxation geospeedometer for volcanic glasses. Chem Geol 125:137–148
Williams H, McBirney AR (1979) Volcanology. Freeman Cooper, San Francisco, pp 1–398
Wohletz K, Heiken G (1992) Volcanology and geothermal energy. Univ California Press, Berkeley, pp 1–432
Zapunnyy SA, Sobolev AV, Bogdanov AA, Slutsky AB, Dmitriev LV, Kunin LL (1989) An apparatus for high-temperature optical research with controlled oxygen fugacity. Geochem Int 26:120–128
Zhang Y, Stolper EM, Wasserburg GJ (1991) Diffusion of water in rhyolitic glasses. Geochim Cosmochim Acia 55:441–456